

# Multiscale image quality measures for defect detection in thin films

A. S. Tolba · Hazem M. Raafat

Received: 26 February 2013 / Accepted: 26 December 2014 / Published online: 30 January 2015  
© Springer-Verlag London 2015

**Abstract** Manufacturing defects in flat surface products such as thin films, paper, foils, aluminum plates, steel slabs, fabrics, and glass sheets result in degradation of the visual quality of the product image. This leads to less satisfied customers, waste of material, and bad company reputation. This research presents a novel application of image visual quality measures such as the multiscale structural similarity index (MS-SSIM). A novel algorithm has been implemented for fast detection and location of defects in many flat surface products. Comparison of the proposed algorithm with the state-of-the-art approaches indicate promising results. A defect detection accuracy of 99.1 % has been achieved with 98.62 % precision, 97.7 % recall/sensitivity, and 100 % specificity. The discriminant power shows how well the MS-SSIM discriminates very effectively between normal and abnormal surfaces. The MS-SSIM has resulted in much better performance than the single-scale SSI approach but at the cost of relatively lower processing speed. The major advantages of the presented approach are as follows: scale invariance, avoiding the problem of parameter selection in the case of the state-of-the-art Gabor filter banks based approach, the higher detection accuracy, and the quasi real-time processing speed.

**Keywords** Automated visual inspection · Defect detection · Multiscale structural similarity index · Computer vision

---

A. S. Tolba (✉)  
Computer Science Department, Mansoura University, Mansoura,  
Egypt  
e-mail: astolba@mans.edu.eg

H. M. Raafat  
Computer Science Department, Kuwait University, Kuwait, Kuwait

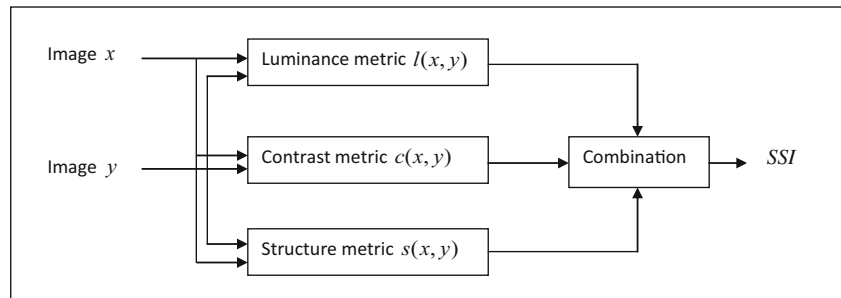
## 1 Introduction

Automated visual surface inspection of industrial products like polymer films is necessary for ensuring film quality. Machine vision inspection of defects relies on efficient algorithms for abnormality detection in real time to cope with the high production speeds. Many algorithms have been recently developed for inspection of fabrics [1–23], paper [24–28], foils [29, 30], and steel slab [31–35]. Most of these algorithms have high computational complexity such as Gabor wavelets, wavelet transform, and Gabor filters. Automation of the visual inspection process saves companies a lot of time and raises the quality of their products by avoiding the subjectivity, slowness of the traditional human-based inspection process. When a defective product reaches the consumer, the company's reputation will be weakened. AVI helps an implementation of good quality control and documentation. Most of the state-of-the-art techniques for defect detection in textiles are computationally demanding which renders them useless for real-time detection of defects during the manufacturing process.

In [36], Gamage and Xie presented a vision system for defect detection in cast films. The system is designed to detect four different types of defects: streaks, coating voids, gels, and wrinkles. The correct defect detection ranges from 87 % for the case of gels to 94 % for the case of streaks. The original gray-level images having resolution of  $800 \times 600$  pixels were first smoothed, low pass filtered, and then thresholded into a binary image. Binary images are then segmented using morphological operators and particle analysis for defect detection and analysis in a second phase.

In [37], Johnson presented a machine vision system for nondestructive visual inspection of polymer electrolyte membranes. Film defects are detected and classified using a neural network into four categories: holes, bubbles, thinning, and gels. The system achieved a classification accuracy of 96.1 % with 1.2 % false alarm rate and 7.1 % escape rate.

**Fig. 1** Structure similarity measurement system

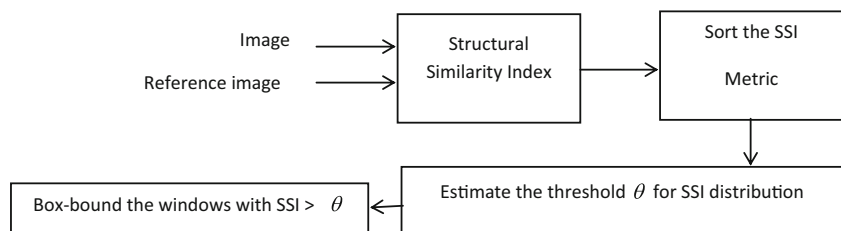


Based on the defect classification results, the operator can take the necessary corrective actions through adjusting the parameters of the manufacturing process. For defect detection, the light regions are highlighted using the top-hat operation, the gray-level image is thresholded using Otsu algorithm, and the morphological operations are used to emphasize blob. On the other hand, dark regions are highlighted using the bottom-hat operation. Nineteen features (size, histogram, topography, geometry, and topology features) are extracted from the segmented defects and then entered into a multilayer perceptron neural network for classification. The major problem in defect classification was the similarity of the characteristics of both bubbles and gels and the characteristics of both holes and thinning defects.

In [38], a system has been presented for defect detection using region growing based image segmentation for classification of defect as conic, bubble, pit, thread, and extraneous substance based on template matching. All defects have been correctly detected with few false alarms. Defects are also classified with an average recall of 95 % and precision of 96 %.

This paper presents a very fast and efficient approach for defect detection and localization in polymer films. The proposed approach relies on a novel algorithm which helps local adaptation of the structural similarity measure that measures the similarity of images of successive windows in a scanned surface. The structural similarity approach renders itself as a very suitable approach for defect detection in flat surfaces since defects are in the first place structural disorders in the making of industrial flat surfaces like thin films, paper, foils, and textiles. Therefore, a fast structural similarity index which is usually used for image quality assessment could be used as a defect detector.

**Fig. 2** Architecture of the structural similarity index (SSI)-based defect detection system

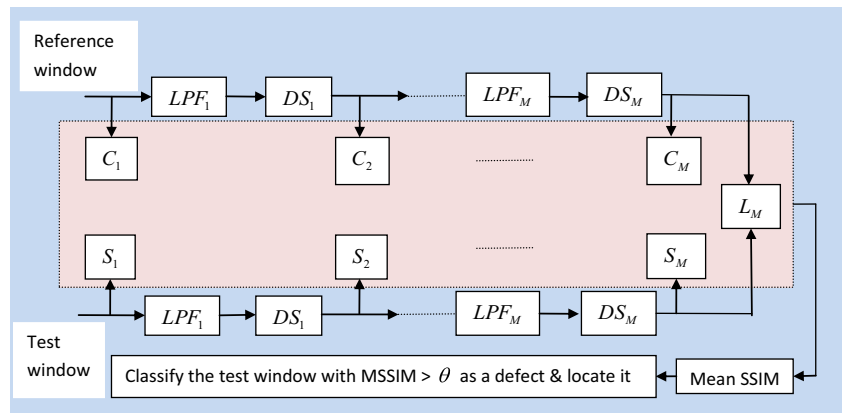


The major contributions of this work are as follows: a novel application of the structural similarity index (SSI) for defect detection in industrial flat surface products and a fast and efficient context based algorithm for defect detection compared to the state of art approaches [1–23] like log-Gabor filters, multiscale multidirectional autocorrelation, Gabor wavelets, and wavelet transform-based techniques. The implemented defect detection technique achieves a comparable accuracy to that achieved by the state-of-the-art approaches in defect detection like log-Gabor wavelets but with lower computational complexity resulting in a 60–100 times faster defect detection system. Figure 1 shows the basic architecture of the proposed defect detection system.

## 2 Structure similarity for defect detection

Visual image quality is a feature of a digital image that indicates its perceived degradation. The most widely applied objective metrics of image quality are the peak signal-to-noise ratio (PSNR) and SSI. There are three categories of objective image quality measures: full reference, reduced reference, or no reference. The traditional full-reference metrics are the mean square error (MSE) and the PSNR. The most recent and powerful metric is the SSI. The SSI metric is based on the characteristics of the human visual system (HVS) in contrary to MSE and PSNR. Figure 1 shows the diagram of the SSI measurement system [39] which is based on modeling of image luminance, contrast, and structure.

**Fig. 3** Architecture of the MS-SSIM-based defect detection system: *LPF* low-pass filtering, *DS* downsampling by 2. Adapted from [41] for defect detection



The SSI is defined in [40] as

$$SSI(x, y) = \frac{(2\mu_x\mu_y + C_1)(2\sigma_{xy} + C_2)}{(\mu_x^2 + \mu_y^2 + C_1)(\sigma_x^2 + \sigma_y^2 + C_2)} \quad (1)$$

where  $\mu_x, \mu_y, \sigma_x,$  and  $\sigma_y$  are the means and standard deviations of both the original and reference images, respectively, and  $C_1$  and  $C_2$  are constants. The three models considered in building the similarity index between the two images  $\mathbf{x}$  and  $\mathbf{y}$  are given by [41]:

$$\text{Luminance} : l(\mathbf{x}, \mathbf{y}) = \frac{2\mu_x\mu_y + C_1}{\mu_x^2 + \mu_y^2 + C_1} \quad (2)$$

$$\text{Contrast} : c(\mathbf{x}, \mathbf{y}) = \frac{2\sigma_x\sigma_y + C_2}{\sigma_x^2 + \sigma_y^2 + C_2} \quad (3)$$

$$\text{Structure} : s(\mathbf{x}, \mathbf{y}) = \frac{\sigma_{xy} + C_3}{\sigma_x\sigma_y + C_3} \quad (4)$$

where  $\mu_x, \sigma_x^2,$  and  $\sigma_{xy}$  are the mean of  $\mathbf{x}$ , the variance of  $\mathbf{x}$ , and the covariance of  $\mathbf{x}$  and  $\mathbf{y}$ , respectively, while  $C_1, C_2,$  and  $C_3$  are constants given by  $C_1=(K_1L)^2, C_2=(K_2L)^2,$  and  $C_3=C_2/2.$   $L$  is the dynamic range for the sample data, i.e.,  $L=255$  for 8-

bit gray-level image and  $K_1 \ll 1$  and  $K_2 \ll 1$  are two scalar constants. Given the above measures, the structural similarity can be computed in [41, 42] as

$$SSI(\mathbf{x}, \mathbf{y}) = [l(\mathbf{x}, \mathbf{y})]^\alpha \cdot [c(\mathbf{x}, \mathbf{y})]^\beta \cdot [s(\mathbf{x}, \mathbf{y})]^\gamma \quad (5)$$

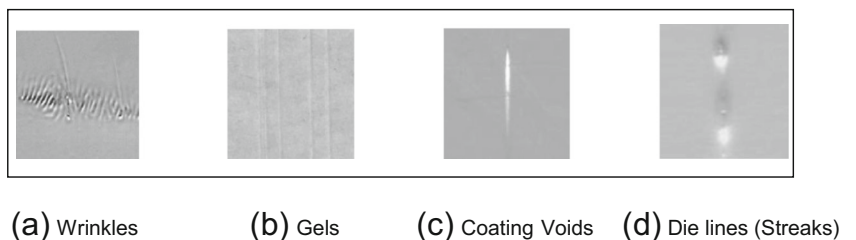
where  $\alpha, \beta,$  and  $\gamma$  define the weight given to each model. Figure 2 shows the architecture of a defect detection system that is based on the SSI. The image of the thin film will be divided into small windows. The SSI is calculated between the reference defect-free window image and the currently scanned window. A suitable threshold level for the SSI is calculated based on the inflection point of the SSI distribution. The scanned window with a SSI above the threshold level is marked as a defective subimage.

The multiscale structural similarity index (MS-SSIM) quality metric, on the other hand, is an extension of the SSIM which computes these measures at various scales and combines them using an equation of the form [41]:

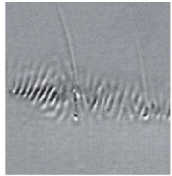
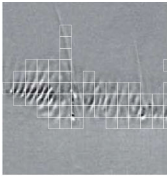
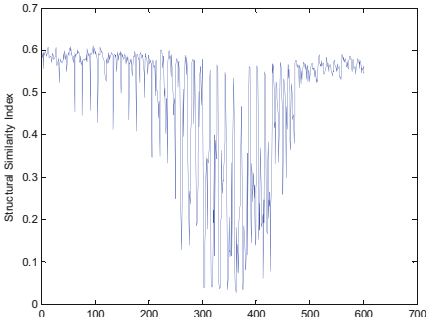

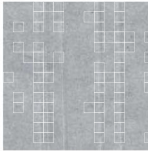
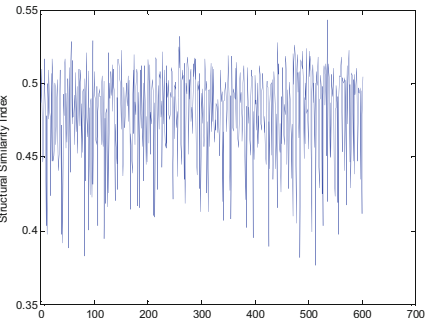


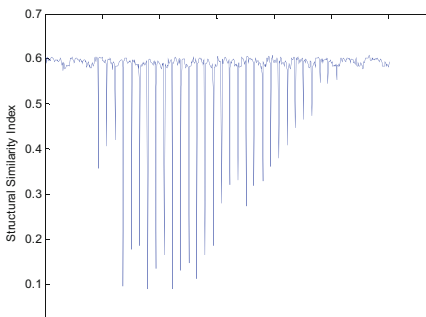
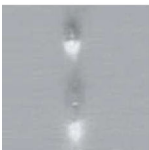
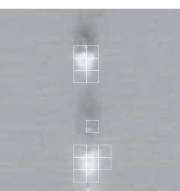
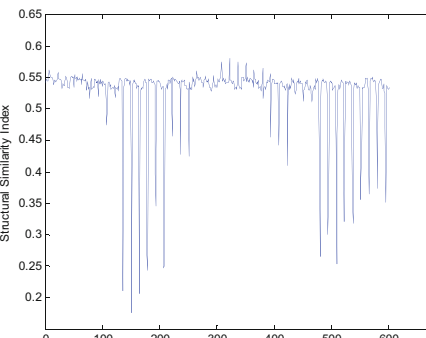
$$MSSSIM(\mathbf{x}, \mathbf{y}) = [l_M(\mathbf{x}, \mathbf{y})]^{\alpha_M} \cdot \prod_{j=1}^M [c_j(\mathbf{x}, \mathbf{y})]^{\beta_j} \cdot [s_j(\mathbf{x}, \mathbf{y})]^{\gamma_j} \quad (6)$$

where  $M$  corresponds to the lowest resolution (i.e., the times of down samplings performed to reduce the image resolution), while  $j=1$  corresponds the original resolution of the image. The architecture of the proposed defect detection system is shown in Fig. 3. Since the performance of the visual

**Fig. 4** Polymer film defects [36]



**Table 1** Defect detection results (A: abnormal block/defect, N: normal block/defect free)

Defect class	Image	Detected defects	SSI distribution									
Wrinkles		 <table border="1" data-bbox="584 485 895 590"> <tr> <td></td> <td>A</td> <td>N</td> </tr> <tr> <td>A</td> <td>52</td> <td>3</td> </tr> <tr> <td>N</td> <td>0</td> <td>141</td> </tr> </table>		A	N	A	52	3	N	0	141	
	A	N										
A	52	3										
N	0	141										
Streaks		 <table border="1" data-bbox="584 821 895 926"> <tr> <td></td> <td>A</td> <td>N</td> </tr> <tr> <td>A</td> <td>69</td> <td>0</td> </tr> <tr> <td>N</td> <td>10</td> <td>117</td> </tr> </table>		A	N	A	69	0	N	10	117	
	A	N										
A	69	0										
N	10	117										
Coating Voids		 <table border="1" data-bbox="584 1199 895 1304"> <tr> <td></td> <td>A</td> <td>N</td> </tr> <tr> <td>A</td> <td>9</td> <td>0</td> </tr> <tr> <td>N</td> <td>1</td> <td>186</td> </tr> </table>		A	N	A	9	0	N	1	186	
	A	N										
A	9	0										
N	1	186										
Gels		 <table border="1" data-bbox="584 1619 895 1724"> <tr> <td></td> <td>A</td> <td>N</td> </tr> <tr> <td>A</td> <td>31</td> <td>2</td> </tr> <tr> <td>N</td> <td>4</td> <td>159</td> </tr> </table>		A	N	A	31	2	N	4	159	
	A	N										
A	31	2										
N	4	159										

inspection of flat surface products relies heavily on the distance between the vision system and the inspected surface,

resolution of the analyzed image has a significant impact on defect detection results. The interaction between defect size

and image resolution is also an important factor. Therefore, using the MS-SSIM metric renders itself a good adaptive measure for defect detection. Figure 3 presents the architecture of a novel system for defect detection based on the MS-SSIM. The architecture is adapted from the MS-SSIM system given in [41] to be applicable for defect detection in thin films. Details about the MS-SSIM could be found in [41, 42]. Each downsampling stage (DS) is preceded by a low-pass filtering (LPF) stage. For defect detection, a defect-free reference image window is successively compared with scanned image windows. A deviation from the defect-free reference window is indicated by a low MS-SSIM value. The mean SSI of all the different scales is calculated and compared to an adaptively calculated threshold limit  $\theta$ .

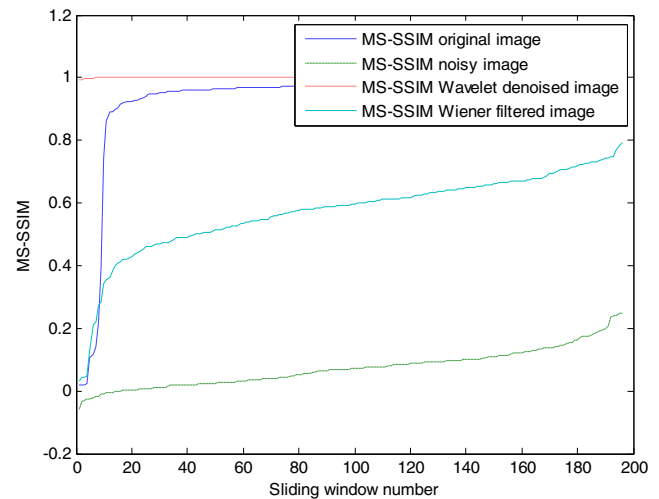


Fig. 5 MS-SSIM variation with filtering approach compared to the original image (coat voids case)

### 3 MS-SSIM-based defect detection algorithm

First, determine the size  $[n_r \times n_c]$  pixels of the whole window acquired by the imaging system, where  $n_r$  is the number of rows and  $n_c$  is the number of columns, then apply the following algorithm:

1. Select a defect reference window  $x$  of size  $[w_w \times w_h]$  pixels, where  $w_w$  is the window width and  $w_h$  is the window height.

2. Initialize the size  $[w_w \times w_h]$  pixels of the sliding test window  $y$ , where  $w_w$  is the window width and  $w_h$  is the window height.
3. Scan the whole test image of the product starting from the top-left corner and ending with bottom-right corner.
4. For each scanning step 3, compute the MS-SSIM( $x,y$ ) of the both the reference window  $x$  and the current window  $y$ .
5. Sort the MS-SSIMs for all the scanned windows.
6. Identify the threshold  $\theta$  of the MS-SSIMs.

Table 2 Wiener filtering/wavelet filtering effect on defect detection

Case	Image	Defect Detection	Image	Defect Detection
Original image				
Original image with Gaussian noise				
Wiener filtered image				
Wavelet based denoising				

**Table 3** Average system performance indicators for SSI approach

Image	Sensitivity	Specificity	Accuracy	Precision	YI	$\rho_+$	$\rho_-$	DP
1	1	1	1	1	1	$\infty$	0	$\infty$
2	0.886	0.988	0.8733	0.939	0.966	71.3	1	3.5
3	0.900	1	0.995	1	0.900	$\infty$	0.1	$\infty$
4	0.945	1	0.9455	1	0.985	$\infty$	0.1	$\infty$
Average	0.9327	0.9970	0.9535	0.9848	0.9627	$\infty$	0.3	$\infty$

- Bound those windows whose MS-SSIM is greater than the threshold value  $\theta$  with a rectangular box, and add them to the set of defect blocks.

Estimation of the appropriate threshold level for the MS-SSIM test is very critical to the success of the presented defect detection system. The average MS-SSIM for a scanned defect-free area is used as a threshold limit for separating defective windows from defect-free windows. The curves shown in Table 1 shows the variation which represents a sharp decrease in the value of MS-SSIM values by the first occurrence of a fabric defect.

#### 4 Defects database

To evaluate the proposed method, a set of images of polymer film defects [36] has been used in our experiments (Fig. 4). The polymer film images were acquired in gray level with a resolution of  $240 \times 232$  pixels. Each sample is scanned with a sliding window of size [ $w_w \times w_h$  pixels] where  $w_h$  is the window width and  $w_h$  is the window height in pixels. The window scans the image with a horizontal shift of  $w_w$  pixels and a vertical shift of  $w_h$ . The following kinds of defects have been tested: gels, streaks, coating voids, wrinkles, structural defect dark areas, light areas, and intensity defects.

#### 5 Experimental results

Experiments were performed on four different classes of defects as shown in Table 1. The first column shows the defect class, and the second column shows the original image. Defect detection and location is shown in column 3 together with the confusion matrix which summaries the test results. It shows the true abnormal (TA), false abnormal (FA), true normal (TN), and false normal (FN) results for each test image. The fourth column shows the distribution of SSI for all the scanned blocks. Blocks which belong to a defective area have small SSI values. The most suitable threshold is found adaptively for each test sample. The most difficult case was that of the

streaks class since the streaks are not highly separable from the background.

#### 6 System robustness to noise

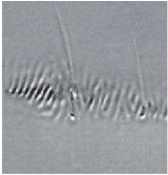
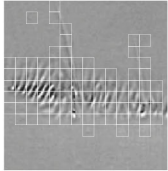
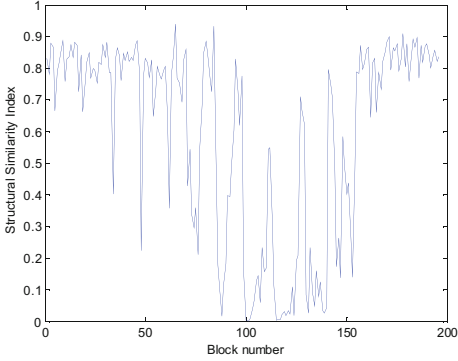

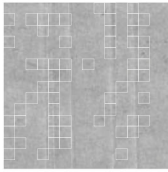
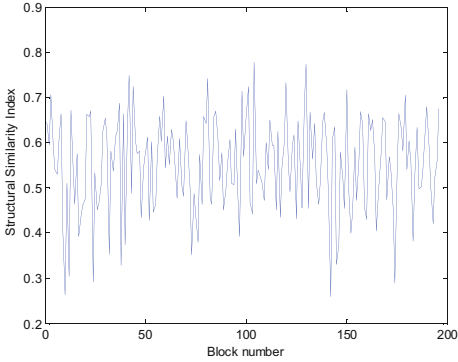


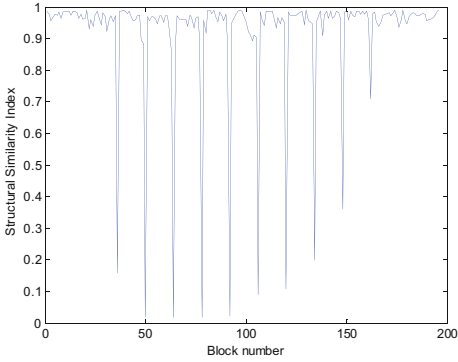
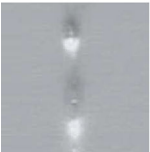
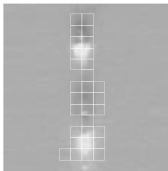
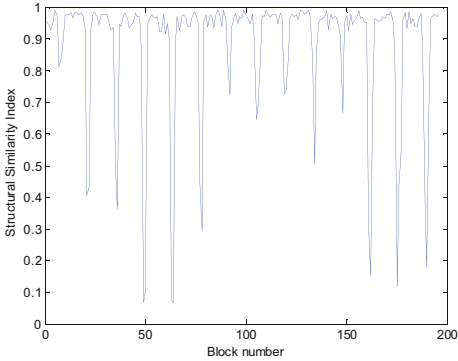
A reliable defect detection system should be robust against any phenomena which might result in false alarms. Noise of the imaging system is one source of false alarms. To remedy this situation, film images are de-noised in a preprocessing phase. Different experiments have been performed to identify the most suitable image de-noising approach for defect detection. Two experiments have been performed using two different filters for image de-noising: Wiener filter [43] and wavelet transform filtering [44]. To evaluate the performance of each filter, the following algorithm has been implemented:

- Add Gaussian noise to the original images.
- Apply the presented defect detection approach to the noisy image.
- Evaluate the defect detection performance based on the accuracy, sensitivity, and precision.
- Apply the de-noising filter.
- Re-evaluate the defect detection performance based on the accuracy, sensitivity, and precision.
- Compare the defect detection performance of steps 3.

To enhance the defect detection capability of the proposed approach in the presence of noise, a linear Wiener filter [43] is applied to the textile image for adaptive noise reduction. The advantage of Wiener filter is that it adapts its smoothing operation with the local gray-level variance. For small gray-level variance, it performs more smoothing and vice versa. The filtering process does not affect neither edges nor high frequencies in the image. Wiener filter is reported to be effective in removing Gaussian noise. The above table shows that the Gaussian noise deteriorates the performance of the MS-SSIM defect detector (second row of the Table 2). A necessary preprocessing step is to use the Wiener filter for de-noising textile images before defect detection. Wavelet denoising failed to enhance the defect detection (fourth row of



**Table 4** Defect detection results (A: abnormal block/defect, N: normal block/defect free)

Defect class	Image	Detected defects	MSSIM distribution									
Wrinkles		 <table border="1" data-bbox="584 499 895 600"> <tr> <td></td> <td>A</td> <td>N</td> </tr> <tr> <td>A</td> <td>52</td> <td>0</td> </tr> <tr> <td>N</td> <td>0</td> <td>145</td> </tr> </table>		A	N	A	52	0	N	0	145	
	A	N										
A	52	0										
N	0	145										
Streaks		 <table border="1" data-bbox="584 888 895 989"> <tr> <td></td> <td>A</td> <td>N</td> </tr> <tr> <td>A</td> <td>69</td> <td>0</td> </tr> <tr> <td>N</td> <td>7</td> <td>120</td> </tr> </table>		A	N	A	69	0	N	7	120	
	A	N										
A	69	0										
N	7	120										
Coating Voids		 <table border="1" data-bbox="584 1276 895 1377"> <tr> <td></td> <td>A</td> <td>N</td> </tr> <tr> <td>A</td> <td>10</td> <td>0</td> </tr> <tr> <td>N</td> <td>0</td> <td>186</td> </tr> </table>		A	N	A	10	0	N	0	186	
	A	N										
A	10	0										
N	0	186										
Gels		 <table border="1" data-bbox="584 1665 895 1766"> <tr> <td></td> <td>A</td> <td>N</td> </tr> <tr> <td>A</td> <td>31</td> <td>0</td> </tr> <tr> <td>N</td> <td>0</td> <td>165</td> </tr> </table>		A	N	A	31	0	N	0	165	
	A	N										
A	31	0										
N	0	165										

**Table 5** Average system performance indicators for MS-SSIM approach

Image	Sensitivity	Specificity	Accuracy	Precision	YI	$\rho_+$	$\rho_-$	DP
1	1	1	1	1	1	$\infty$	0	$\infty$
2	0.908	1	0.964	0.945	0.9079	$\infty$	0.1	$\infty$
3	1	1	1	1	1	$\infty$	0	$\infty$
4	1	1	1	1	1	$\infty$	0	$\infty$
Average	0.9770	1	0.9910	0.9862	0.9970	$\infty$	0.0250	$\infty$

Table 2) since the process of setting a threshold will be very difficult.

Figure 5 shows an example for the variation of MS-SSIM with noise, Wiener filtering, and wavelet filtering compared to the case of a noise-free image. It can be concluded that Wiener filtering results in a distribution of MS-SSIM which is nearly similar to that of the original noise-free image and does not need any change of the threshold limit to achieve approximately the same level of performance. Results of wavelet filtering need changing the threshold limit, and it will be unstable.

## 7 Performance evaluation

Evaluating the performance of the proposed defect detection approach is a major factor that requires careful consideration. The percentage of correct detection (PCD) generally has been used as a measure of performance of most defect detection approaches. However, there exists a variety of measures for judging the performance of classifiers. In our work, we have considered the following four performance measures as discussed in detail in [45–48]:

$$\text{Precision} = \frac{TA}{(TA + FA)} \quad (7)$$

$$\text{Recall (sensitivity)} = \frac{TA}{(TA + FN)} \quad (8)$$

$$\text{Specificity} = \frac{TN}{(TN + FA)} \quad (9)$$

$$\text{Accuracy} = \frac{(TA + TN)}{(TA + TN + FA + FN)} \quad (10)$$

All of the above quantities normally are expressed as percentages. The various terms appearing in the above equations are as follows: TA, FA, FN, and TN. These terms can be obtained easily from the confusion matrix related to a defect detection or classification task. The meanings associated with the above measures are given in the following in the context of defect detection tasks:

1. Precision indicates the percentage of correct abnormal classifications.
2. Recall (sensitivity) indicates the percentage of samples that were classified as abnormal and which were labeled as abnormal (i.e., the true abnormality rate).
3. Specificity indicates the percentage of samples that were classified as normal and which were labeled as normal (i.e., the true normality rate).
4. Accuracy indicates the PCD.

Youden's index (YI) evaluates the classifier performance to a finer degree with respect to both classes. A higher positive value of  $\rho_+$  means a better performance on the abnormal texture class. A higher negative value of  $\rho_-$  means a better performance on the normal texture class. The DP evaluates how well a classifier discriminates between normal (N) and abnormal (A) surfaces. The classifier performance is poor if  $DP < 1$ , limited if  $DP < 2$ , fair if  $DP < 3$ , and good—in other cases [31]. An infinite value of the discriminating power indicates excellent performance in discrimination between normal and abnormal textures. The average performance of the proposed system has been tested on four samples with 196 sliding windows. The test results given in Table 3 show acceptable performance.

The above performance indicators have been calculated based on the confusion matrix of every sample as shown in Table 3. The SSI-based defect detection resulted in 0.9327 sensitivity, 0.9970 specificity, 0.977 Youden's index, 0.9535 accuracy, and 0.9848 precision. Higher positive and lower

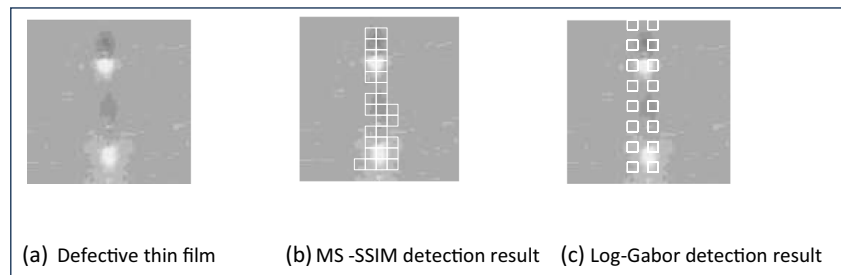
**Table 6** System performance for the morphological operators and particle analysis approach presented by Gamage and Xie [36]

Image	Accuracy of morphological processing [23]	SSI accuracy (%)	MS-SSIM accuracy (%)
Gels	87%	100	100
Streaks	94%	87.43	96.4
Wrinkles	N/A	94.90	100
Coating voids	N/A	94.55	99.1
Average	N/A	95.35	99.1

Source: [36]



**Fig. 6** MS-SSIM detection results compared to the log-Gabor detection results (gels case)

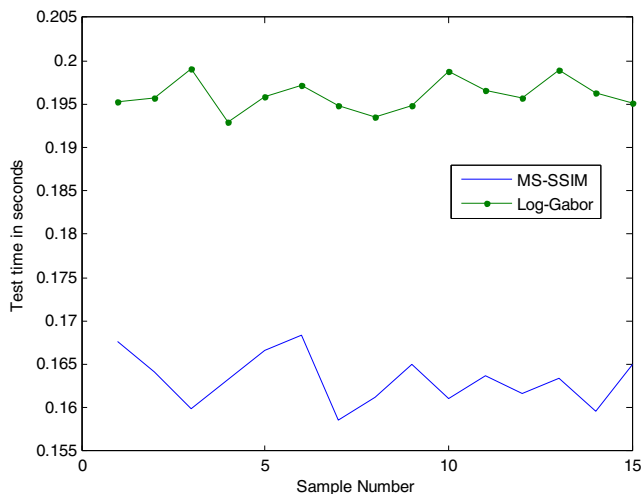


negative likelihood ratios for a certain sample mean better performance on positive and negative classes, respectively [47]. The DP indicates that the proposed algorithm differentiates very well between normal and abnormal texture areas. The higher positive values of  $\rho_+$  indicate good performance on the abnormal texture class. The higher negative value of  $\rho_-$  means good performance on the normal texture class. Application of the MS-SSIM resulted in enhanced system performance indicators as could be seen in Tables 4 and 5.

## 8 Comparison with the other approaches

There are few published results on defect detection in thin films. For comparison purposes, the MS-SSIM and SSI approaches resulted in better performance compared to the performance reported in [36]. The main emphasis in [36] was about the design of a real-time system. Results were only reported about defects of the two classes: gels and streaks (Table 6).

Figure 6 shows the superior detection results of the MS-SSIM approach compared to LG-Gabor approach [3]. The average processing time for detection of defects of 15 samples using the MS-SSIM approach is about 83.27 % of the time elapsed by the LG approach as shown in Fig. 7.



**Fig. 7** Test time of both MS-SSIM and log-Gabor defect detection approaches

## 9 Conclusions

In this paper, a novel automated defect detection approach has been proposed using the MS-SSIM. Using the MS-SSIM metric as a homogeneity measure, defects could be detected and localized. A defect detection accuracy of 99.1 % has been achieved with 98.62 % precision, 97.7 % recall/sensitivity, and 100 % specificity. The discriminant power shows how well the MS-SSIM discriminates very effectively between normal and abnormal surfaces. The experimental results show that the proposed approach results in excellent defect detection performance compared to the state-of-the-art approaches. The MS-SSIM has resulted in much better performance than the single-scale SSI approach but at the cost of relatively lower processing speed. The major advantages of the presented approach are avoiding the problem of parameter selection in the case of the state of the art Gabor filter-based approach, the higher detection accuracy, and the quasi real-time processing speed. Future work will be concerned with parallel implementation using the NVIDIA GPU board for real-time defect detection. Testing on much larger ranges of samples not previously seen by the operators would be needed to establish statistically representative performance figures.

**Acknowledgments** The authors would like to thank their respective universities for providing the opportunity and facilities to undertake this research. They also would like to thank Gamage, P. [36] for giving us the permission to use the thin film images used in the experiments.

## References

1. Ngan HYT, Pang GKH, Yung NHC (2011) Automated fabric defect detection—a review. *Image Vis Comput* 29(7):442–458
2. Tsai D-M, Chen M-C, Li W-C, Chiu W-Y (2012) A fast regularity measure for surface defect detection. *Mach Vis Appl* 23(5):869–886
3. Tolba AS, Atwan A, Amanneddine N, Mutawa AM, Khan HA (2010) Defect detection in flat surface products using log-Gabor filters. *Int J Hybrid Intell Syst* 7(3):187–201
4. Hamid Alimohamadi, Alireza Ahmadyfard, Esmail Shojaei (2009) Defect detection in textiles using morphological analysis of optimal Gabor wavelet filter response. *ICCAE, International Conference on Computer and Automation Engineering*, pp. 26–30
5. Kumar A, Member, IEEE, Pang GKH (2002) Defect detection in textured materials using Gabor filters. *IEEE Trans Ind Appl* 38(2): 425–439

6. K. L. Mak, and P. Peng, Detecting defects in textile fabrics with optimal Gabor filters, in World Academy of Science, Engineering and Technology 13 2008
7. Mak KL, Peng P, Yiu KFC (2009) Fabric defect detection using morphological filters. *Image Vis Comput* 27:1585–1592
8. Tolba AS (2012) A novel multiscale-multidirectional autocorrelation approach for defect detection in homogeneous flat surfaces. *Mach Vis Appl* 23(4):739–750
9. Escofet J, Navarro R, Milla'n MS (1998) Detection of local defects in textile webs using Gabor filters. *Opt Eng* 37(8):2297–2307
10. K. N. Sivabalan, D. Gnanadurai (2011) Efficient defect detection algorithm for gray level digital images using Gabor wavelet filter and Gaussian filter. *Int J Eng Sci Technol (IJEST)*, Vol. 3 No. 4
11. V Asha, N U Bhajantri, and P Nagabhushan, Automatic detection of texture defects using texture-periodicity and Gabor wavelets. <http://arxiv.org/pdf/1212.1329>
12. Arivazhagan S, Ganesan L, Bama S (2006) Fault segmentation in fabric images using Gabor wavelet transform. *Mach Vis Appl* 16(6): 356–363
13. Sajid T, Ali B (2012) Fabric defect detection in textile images using Gabor filter. *IOSR J Electric Electron Eng* 3(2):33–38
14. Narges Heidari, Reza Azmi & Boshra Pishgoo (2011) Fabric textile defect detection, by selecting a suitable subset of wavelet coefficients, through genetic algorithm. *Int J Image Process* 5(1):701–710
15. Rashmi S Deshmukh, P R Deshmukh and Abhijit M Taley (2012) Comparison analysis for efficient defect detection algorithm for gray level digital images using median filters Gabor filter and ICA. *Int J Adv Res Comput Sci Software Eng* 2(1)
16. Kumar A (2008) Computer vision-based fabric defect detection: a survey. *IEEE Trans Ind Electron* 55(1):348–363
17. Tolba AS, Khan HA, Mutawa AM, Alsalem SM (2010) Decision fusion for visual inspection of textiles. *Text Res J* 80(19):2094–2106
18. Mahajan P.M., Kolhe S.R. and Patil P.M.A (2009) Review of automatic fabric defect detection techniques. *Adv Comput Res* 1(2):18–29
19. Tolba AS (2011) Neighborhood-preserving cross correlation for automated visual inspection of fine-structured textile fabrics. *Textile Res* 81(19):2033–2012
20. Shanbhag PM, Deshmukh MP, Suralkar SR (2012) Overview: methods of automatic fabric defect detection. *Global J Eng Des Technol* 1(2):42–46
21. R. S. Sabeenian, M. E. Paramasivam, P. M. Dinesh (2012) Computer vision based defect detection and identification in handloom silk fabrics. *Int J Comput Applic* 42(17):41–48
22. Mahajan P.M., Kolhe S.R. and Patil P.M.A (2009) A review of automatic fabric defect detection techniques. *Adv Comput Res* 1(2):18–29
23. Xiem X (2008) A review of recent advances in surface defect detection using texture analysis techniques. *Electronic Lett Comput Vision Imag Anal* 7(3):1–22
24. Iivarinen, J., Rauhamaa, J. (1998) Surface inspection of web materials using the self-organizing map. In: Casasent, D.P. (ed.) *Proceedings of the SPIE*, vol. 3522, Intelligent Robots and Computer Vision XVII: Algorithms, Techniques, and Active Vision, pp. 96–103
25. Turtinen M, Pietik`ainen M and Silven O (2005) Visual characterization of paper using isomap and local binary patterns, MVA2005 IAPR Conference on Machine Vision Applications, pp. 210–213, May 16–18, Tsukuba Science City, Japan
26. Iivarinen J and Pakkanen J (2002) Content-based retrieval of defect images, *Proceedings of ACIVS 2002 (Advanced Concepts for Intelligent Vision Systems)*, Ghent, Belgium, September 9–11
27. Shubo, Q, Shuai, G, Tongxing, Z. Research on paper defects recognition based on SVM, 2010 WASE Int Conference Inform Eng
28. Rauhamaa J, and Reinius, R. Paper web imaging with advanced defect classification, TAPPI Paper Summit 2002
29. Zhai M, Shan F, Shimin G, Xie Z, Luo X (2011) Defect detection in aluminum foil by measurement-residual-based chi-square detector. *Int J Adv Manuf Technol* 53:661–667
30. Lin S-W, Chou S-Y, Chen S-C (2006) Irregular shapes classification by back-propagation neural networks. *Int J Adv Manuf Technol*. doi: 10.1007/s00170-006-0667-3
31. Jia H, Murphey Y L, Shi J, Chang T-S. (2004) An intelligent real-time vision system for surface defect detection, *ICPR* (3):239–242
32. Wu Xiu-yong, Xu Ke and Xu Jin-wu (2008) Application of undecimated wavelet transform to surface defect detection of hot rolled steel plates, 2008 Congress on Image and Signal Processing
33. Liu Weiwei, Yan Yunhui, Li Jun, Zhang Yao, Sun Hongwei (2008) Automated on-line fast detection for surface defect of steel strip based on multivariate discriminant function second international symposium on intelligent information technology application. *IEEE*
34. Mohammad Reza Yazdchi, Arash Golibagh Mahyari, Ali Nazeri, Detection and Classification of Surface Defects of Cold Rolling Mill Steel Using Morphology and Neural Network, *CIMCA 2008, IAWTIC 2008, and ISE 2008*
35. Jia H, Murphey Y L, Shi J, Chang T-S. An intelligent real-time vision system for surface defect detection, proceedings of the 17th International Conference on Pattern Recognition (ICPR'04)
36. Gamage P, Xie S (2008) A real-time vision system for defect inspection in cast extrusion manufacturing process. *Int J Adv Manuf Technol* 40:144–156
37. Johnson, J T Defect and thickness inspection system for cast thin films using machine vision and full-field transmission densitometry, MSc. Thesis, School of George W. Woodruff School of Mechanical Engineering Georgia Institute of Technology, December 2009
38. Young-Geun Y, Seok Lyong L, Chin-Wan C, Sang Hee K (2008) An effective defect inspection system for polarized film images using image segmentation and template matching techniques. *Comput Ind Eng* 5:567–583
39. Shang X (2006) Structural similarity based image quality assessment: pooling strategies and applications to image compression and digit recognition. M.Sc. Thesis Presented to the Faculty of the Graduate School of The University of Texas at Arlington, August
40. Z. Wang and A. C. Bovik (2006) Modern image quality assessment. Morgan and Claypool
41. Zhou Wang1, Eero P. Simoncelli1 and Alan C. Bovik (2003) Multi-scale structural similarity for image quality assessment, *Proceedings of the 37th IEEE Asilomar conference on signals, systems and computers*, Pacific Grove, CA, Nov. 9–12
42. Z. Wang, A. C. Bovik, H. R. Sheikh, and E. P. Simoncelli, "Image quality assessment: From error measurement to structural similarity," *IEEE Trans. Image Processing*, vol. 13, Jan. 2004
43. Gonzalez RC, Woods RE (1992) *Digital image processing*. Addison-Wesley, New York
44. Donoho DL (1995) De-noising by soft-thresholding. *IEEE Trans Inf Theory* 41(3):613–662
45. D. G. Altman and J. M. Bland (1994) Statistics notes: diagnostic tests. 1: Sensitivity and specificity. *BMJ* 308(6943):1552
46. Lu Z et al (2004) Predicting subcellular localization of proteins using machine-learned classifiers. *Bioinformatics* 20(4):547–556
47. R. Eisner et al. (2005) Improving protein function prediction using the hierarchical structure of the gene ontology, *IEEE Symposium on Computational Intelligence in Bioinformatics and Computational Biology*
48. Sokolova M, Japkowicz N, Szpakowicz S (2006) Beyond accuracy, F-score and ROC: a family of discriminant measures for performance evaluation. *Australian conference on artificial intelligence*, Vol. 4304. LNCS, Germany, pp: 1015–1021